AJNR

High-Resolution Surface-Coil Imaging of Lumbar Disk Disease

Robert R. Edelman, Gregory M. Shoukimas, David D. Stark, Kenneth R. Davis, Paul F. J. New, Sanjay Saini, Daniel I. Rosenthal, Gary L. Wismer and Thomas J. Brady

AJNR Am J Neuroradiol 1985, 6 (4) 479-485
http://www.ajnr.org/content/6/4/479

High-Resolution Surface-Coil Imaging of Lumbar Disk Disease

Robert R. Edelman[1]
Gregory M. Shoukimas
David D. Stark
Kenneth R. Davis
Paul F. J. New
Sanjay Saini
Daniel I. Rosenthal
Gary L. Wismer
Thomas J. Brady

Seventeen patients with lumbar disk disease were studied using a prototype magnetic resonance (MR) surface coil. The high signal-to-noise ratio achieved with the surface coil permitted increases in spatial resolution to 0.9 × 0.9 mm in-plane resolution with 5 mm slice thickness. The surface coil was also compatible with multiplanar, multiecho imaging techniques. The spatial resolution achieved in this study was nearly equivalent to that achieved by state-of-the-art computed tomographic (CT) scanners, and MR showed a superior range of soft-tissue contrast. One significant limitation of MR was its inability to demonstrate small calcifications. Nevertheless, MR imaging provided diagnostic information comparable to CT or myelography in a completely noninvasive manner. With further technical advances, MR is likely to become the initial procedure of choice for evaluating patients with suspected lumbar disk disease.

Preliminary studies using conventional magnetic resonance (MR) imaging techniques have demonstrated several unique advantages over computed tomography (CT) and myelography in evaluating lumbar disk disease [1–4]. For example, MR is free of the x-ray beam-hardening artifacts that limit CT. In addition to cross-sectional anatomic detail, MR tissue characteristics allow identification of the degenerated nucleus pulposus [3]. Unfortunately, when conventional radiofrequency (RF) whole-body saddle coils are used, low signal-to-noise (S/N) ratios severely limit achievable anatomic resolution, precluding routine clinical application. The use of a prototype surface coil has increased S/N ratios and spatial resolution. The incorporation of plane selection oriented parallel to the disk with multiplanar imaging [5, 6] has allowed application of MR imaging of the lumbar spine in a routine clinical setting. In this study these new MR techniques are compared with CT and myelography in patients with lumbar disk disease.

Subjects and Methods

Seventeen patients aged 21–60 years were studied with MR at Massachusetts General Hospital. Fourteen of the patients were referred for MR study because CT or myelography performed within the previous 2 weeks demonstrated lumbar disk disease. Three other patients were selected to have MR as the initial study because of clinical symptoms; all three were subsequently proven by CT to have lumbar disk disease. In 10 patients operative results confirmed the CT and myelographic findings. Patients with prior back surgery were excluded from this study.

MR examinations were performed with a Technicare superconducting magnet operated at 0.6 T. Similar systems have been described in detail [7]. A 20-cm-diam prototype two-turn surface coil was used for all patients. The coil was shielded with copper on its sides and bottom to minimize RF coupling with the body coil, which was not removed during imaging. During the course of this study, the surface coil was used as both the RF transmitter and receiver. Standard multislice, multiecho acquisition techniques were completely compatible with this coil configuration. Total setup time for the surface coil was 3 min. Patients were positioned supine with their knees flexed. The midlumbar spine was centered over the surface

This article appears in the July/August 1985 issue of *AJNR* and the June 1985 issue of *AJR*.

Received December 24, 1984; accepted February 20, 1985.

This work was supported in part by Technicare Corp., Solon, OH.

T. J. Brady is the recipient of a research career development award from the National Cancer Institute, Department of Health and Human Services, 1K04CA00848–02.

[1] All authors: Radiology, Massachusetts General Hospital, Boston, MA 02114. Address reprint requests to R. R. Edelman.

***AJNR* 6:479–485, July/August 1985**
0195–6108/85/0604–0479

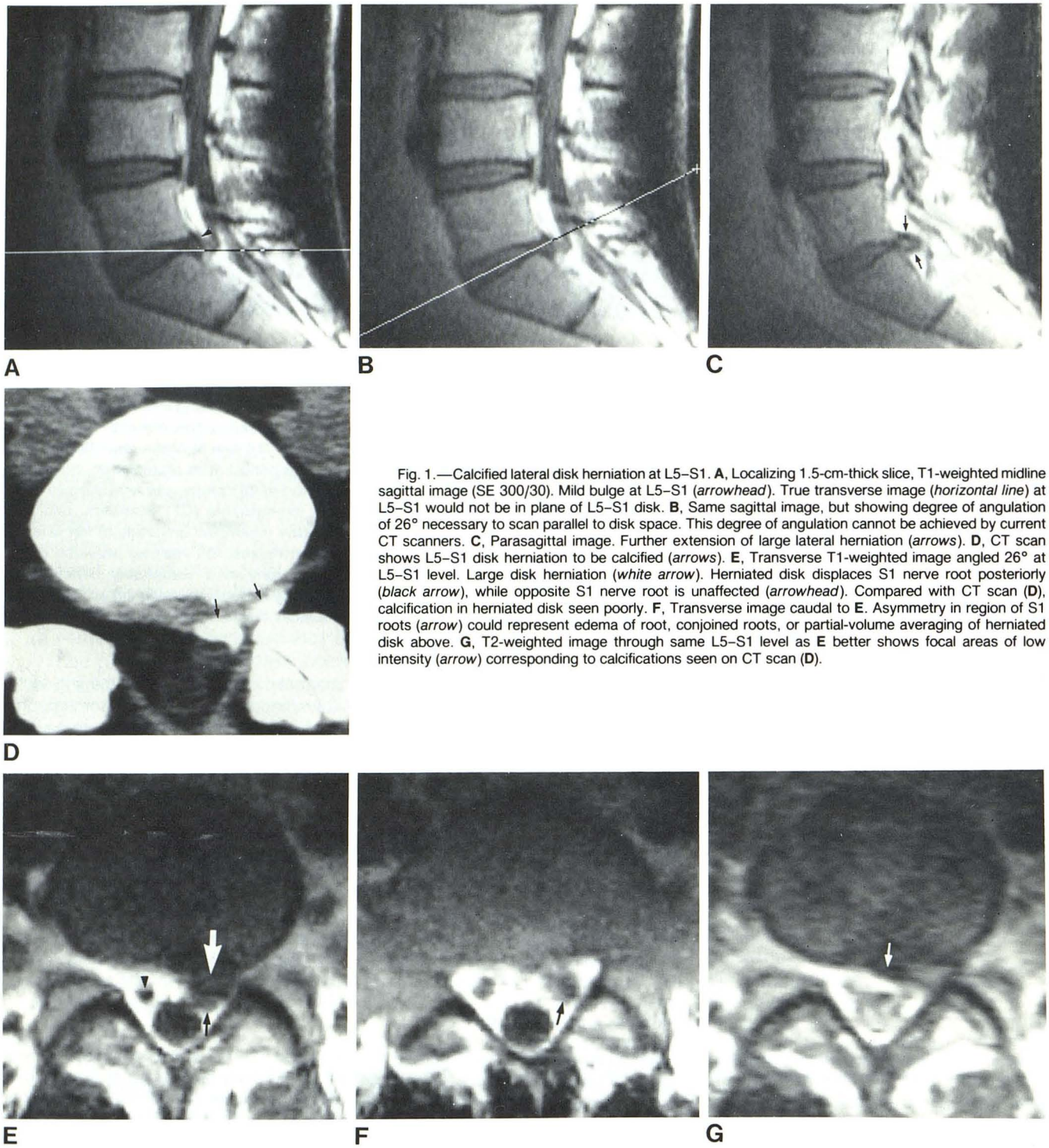

Fig. 1.—Calcified lateral disk herniation at L5–S1. **A**, Localizing 1.5-cm-thick slice, T1-weighted midline sagittal image (SE 300/30). Mild bulge at L5–S1 (*arrowhead*). True transverse image (*horizontal line*) at L5–S1 would not be in plane of L5–S1 disk. **B**, Same sagittal image, but showing degree of angulation of 26° necessary to scan parallel to disk space. This degree of angulation cannot be achieved by current CT scanners. **C**, Parasagittal image. Further extension of large lateral herniation (*arrows*). **D**, CT scan shows L5–S1 disk herniation to be calcified (*arrows*). **E**, Transverse T1-weighted image angled 26° at L5–S1 level. Large disk herniation (*white arrow*). Herniated disk displaces S1 nerve root posteriorly (*black arrow*), while opposite S1 nerve root is unaffected (*arrowhead*). Compared with CT scan (**D**), calcification in herniated disk seen poorly. **F**, Transverse image caudal to **E**. Asymmetry in region of S1 roots (*arrow*) could represent edema of root, conjoined roots, or partial-volume averaging of herniated disk above. **G**, T2-weighted image through same L5–S1 level as **E** better shows focal areas of low intensity (*arrow*) corresponding to calcifications seen on CT scan (**D**).

coil, and positioning was checked by obtaining a single image in the sagittal plane. This initial image was obtained using an image matrix of 256 × 128 elements, yielding an in-plane spatial resolution of 1.8 × 0.9 mm; slice thickness was set at 1.5 cm. Spin-echo (SE) technique with a repetition time (TR) of 300 msec, an echo time (TE) of 30 msec, and two signal averages (SE 300/30/2) allowed localization of L2–S1 in 1.1 min. Once patient positioning was confirmed, in-plane spatial resolution was increased to 0.9 × 0.9 mm by using a 256 × 256 element image matrix and reducing slice thickness to 5 mm. Using this high-resolution technique, multislice acquisition was pos-

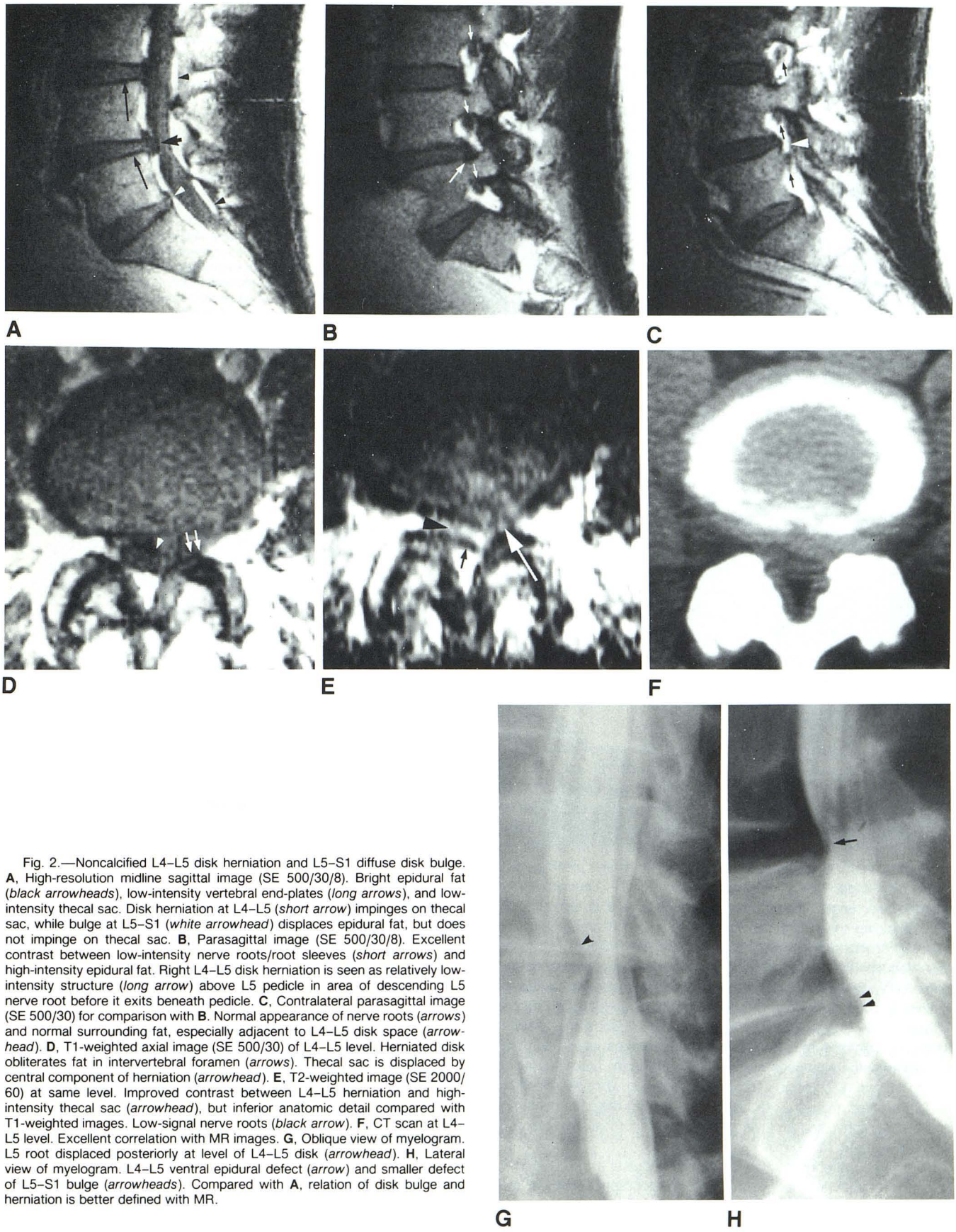

Fig. 2.—Noncalcified L4–L5 disk herniation and L5–S1 diffuse disk bulge. **A**, High-resolution midline sagittal image (SE 500/30/8). Bright epidural fat (*black arrowheads*), low-intensity vertebral end-plates (*long arrows*), and low-intensity thecal sac. Disk herniation at L4–L5 (*short arrow*) impinges on thecal sac, while bulge at L5–S1 (*white arrowhead*) displaces epidural fat, but does not impinge on thecal sac. **B**, Parasagittal image (SE 500/30/8). Excellent contrast between low-intensity nerve roots/root sleeves (*short arrows*) and high-intensity epidural fat. Right L4–L5 disk herniation is seen as relatively low-intensity structure (*long arrow*) above L5 pedicle in area of descending L5 nerve root before it exits beneath pedicle. **C**, Contralateral parasagittal image (SE 500/30) for comparison with **B**. Normal appearance of nerve roots (*arrows*) and normal surrounding fat, especially adjacent to L4–L5 disk space (*arrowhead*). **D**, T1-weighted axial image (SE 500/30) of L4–L5 level. Herniated disk obliterates fat in intervertebral foramen (*arrows*). Thecal sac is displaced by central component of herniation (*arrowhead*). **E**, T2-weighted image (SE 2000/60) at same level. Improved contrast between L4–L5 herniation and high-intensity thecal sac (*arrowhead*), but inferior anatomic detail compared with T1-weighted images. Low-signal nerve roots (*black arrow*). **F**, CT scan at L4–L5 level. Excellent correlation with MR images. **G**, Oblique view of myelogram. L5 root displaced posteriorly at level of L4–L5 disk (*arrowhead*). **H**, Lateral view of myelogram. L4–L5 ventral epidural defect (*arrow*) and smaller defect of L5–S1 bulge (*arrowheads*). Compared with **A**, relation of disk bulge and herniation is better defined with MR.

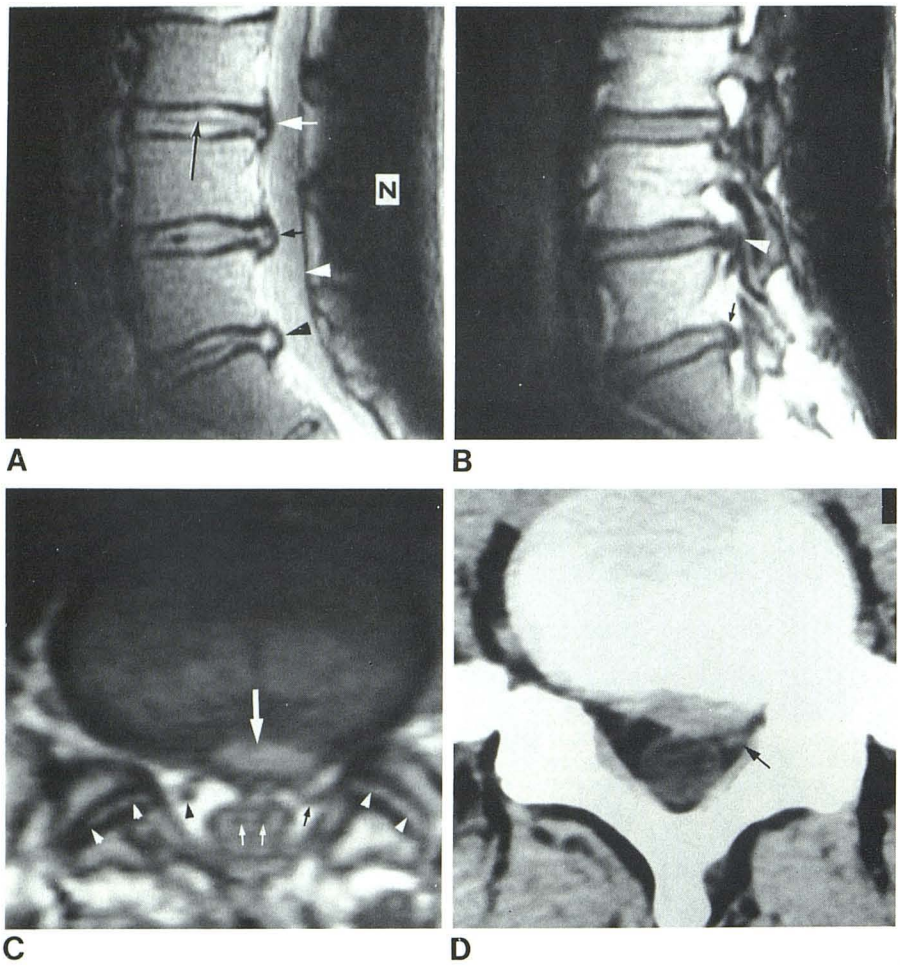

Fig. 3.—Multiple disk herniations and bulges. **A**, T2-weighted midline sagittal image (SE 2000/60). Increased signal from CSF (*white arrowhead*) resulting in MR "myelogram." Small disk bulge at L3–L4 (*white arrow*) is well demonstrated despite paucity of epidural fat at this level. Larger extradural defects at L4–L5 (*short black arrow*) and L5–S1 (*black arrowhead*). Normal thin low-signal line through center of nucleus pulposus (*long black arrow*). Dark band of low ("null") signal (N) is from RF inhomogeneity. **B**, T1-weighted parasagittal image (SE 500/30). Extensive displacement of epidural fat at L4–L5 (*arrowhead*). At L5–S1, herniated disk causes less posterior displacement of epidural fat (*arrow*). **C**, SE 2000/30 axial image through L5–S1. Moderately high signal intensity of herniation (*large white arrow*) encroaching on fat in region of nerve root sleeve (*black arrow*). Opposite S1 nerve root is unaffected (*black arrowhead*). Low signal suggests nerve roots within thecal sac (*small white arrows*) and high signal intensity from synovial fluid within facet joints (*white arrowheads*). **D**, CT at L5–S1. Excellent correlation with MR at L5–S1 level. Displaced S1 root on right (*arrow*).

sible with 1 mm gaps between slices. Similar techniques have been described for use with conventional circumferential RF coils [8].

After localization, 11 multislice sagittal images were obtained in 18 min using an SE 500/30 sequence with eight signal averages. On the basis of the findings on these high-resolution sagittal images, a stack of 11 transverse images was obtained at the level of the suspected abnormality with oblique angulation to orient the image plane parallel to the disk space, as is common practice in CT. Techniques for oblique (Euler angle) imaging have been described in detail [5, 6]. After obtaining these high-resolution "T1-weighted" images in two planes of section, SE 2000/30,60/4 or 2000/60,120/4 double-echo pulse sequences were used for purposes of tissue characterization. These "T2-weighted" images were obtained in either the sagittal or transverse plane to further characterize pathology identified on the "T1-weighted" images. Because of the longer TR times necessary to obtain T2-weighted images, fewer signal averages were used and spatial resolution was decreased to 1.8 × 0.9 mm. To limit imaging time to 18 min, S/N ratios and spatial resolution were sacrificed on the T2-weighted images. Total time for setup, acquisition, reconstruction, photography, and archival of a complete lumbar spine examination was about 75–90 min.

MR images were interpreted by two radiologists (K. R. D. and P. F. J. N.) without knowledge of CT or myelographic findings. MR findings were then compared with results of CT, myelography, and/or surgery.

Results

Twenty-nine disk herniations or bulges were identified in our 17 patients. Nineteen focal herniations and 10 diffuse disk bulges were diagnosed by CT, myelography, and/or surgery. All 29 abnormal disks were detected on the initial sagittal MR images. The axial scans correctly differentiated between 19 disk herniations and 10 disks with diffuse bulging only. However, a free fragment was not detected in one patient. All of the disks shown to be normal by MR were normal by CT and/or myelography.

Sagittal images demonstrated at least three (L3–L4, L4–L5, and L5–S1) disk levels simultaneously (figs. 1A–1C). Epidural fat, which has a relatively short T1 and long T2, appeared as the highest-intensity tissue on both the T1- and T2-weighted images used in this study (fig. 2). The cortical bone of the vertebral end-plates and posterior elements, as well as the ligamentous structures, are characterized by very low mobile proton density and therefore appear black on all sequences studied (fig. 2A). The outer fibers of the normal anulus fibrosus, seen as a dark ring around the nucleus pulposus, were flat or concave posteriorly. The cancellous bone of the superior and inferior facets was of relatively high intensity due to fat-containing marrow, while the surrounding

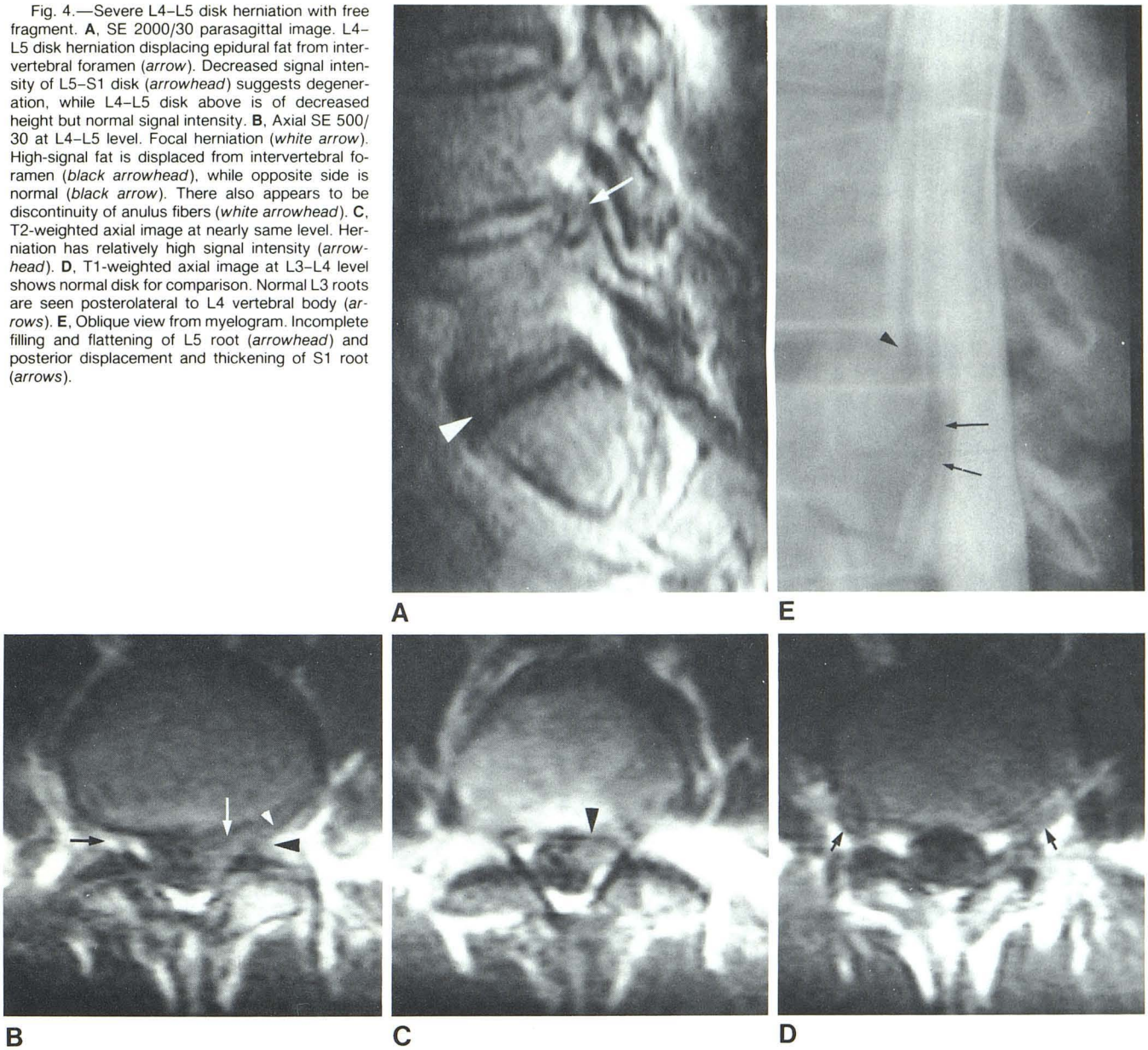

Fig. 4.—Severe L4–L5 disk herniation with free fragment. **A**, SE 2000/30 parasagittal image. L4–L5 disk herniation displacing epidural fat from intervertebral foramen (*arrow*). Decreased signal intensity of L5–S1 disk (*arrowhead*) suggests degeneration, while L4–L5 disk above is of decreased height but normal signal intensity. **B**, Axial SE 500/30 at L4–L5 level. Focal herniation (*white arrow*). High-signal fat is displaced from intervertebral foramen (*black arrowhead*), while opposite side is normal (*black arrow*). There also appears to be discontinuity of anulus fibers (*white arrowhead*). **C**, T2-weighted axial image at nearly same level. Herniation has relatively high signal intensity (*arrowhead*). **D**, T1-weighted axial image at L3–L4 level shows normal disk for comparison. Normal L3 roots are seen posterolateral to L4 vertebral body (*arrows*). **E**, Oblique view from myelogram. Incomplete filling and flattening of L5 root (*arrowhead*) and posterior displacement and thickening of S1 root (*arrows*).

cortical bone had a very low intensity. On T2-weighted images, the facet joint space itself was identified as a high-intensity line due to the presence of synovial fluid (fig. 3C).

The nerve roots/root sheaths are seen as low-intensity structures on both T1- and T2-weighted images. This generally allowed good demonstration of the nerve roots and root sheaths in the neural foramina on the parasagittal images, particularly on the high-resolution T1-weighted sequences (figs. 2B and 2C). The cerebrospinal fluid (CSF)–containing thecal sac demonstrated low signal on T1-weighted images and a progressive increase in signal on T2-weighted images.

On the more T2-weighted images (SE 2000/30 or SE 2000/60) the individual nerve roots of the cauda equina could be seen as low-intensity structures within the bright CSF (fig. 3C). T2-weighted sequences were particularly useful for enhancing contrast between the intervertebral disk and thecal sac when there was a paucity of epidural fat (fig. 3A), providing an MR "myelogram."

The normal nucleus pulposus demonstrated intermediate signal intensity on T1-weighted images and higher intensity as T2 weighting increased. On sagittal images, the nucleus pulposus was divided by a central line of low signal intensity (fig. 3A), possibly representing dense fibrous tissue that normally divides the nucleus during the second decade of life [9]. Herniated disk material appeared similar or slightly lower in intensity compared with the nucleus pulposus on both T1- and T2-weighted sequences in most cases but occasionally was higher in intensity (fig. 3C). Disk herniation had a very

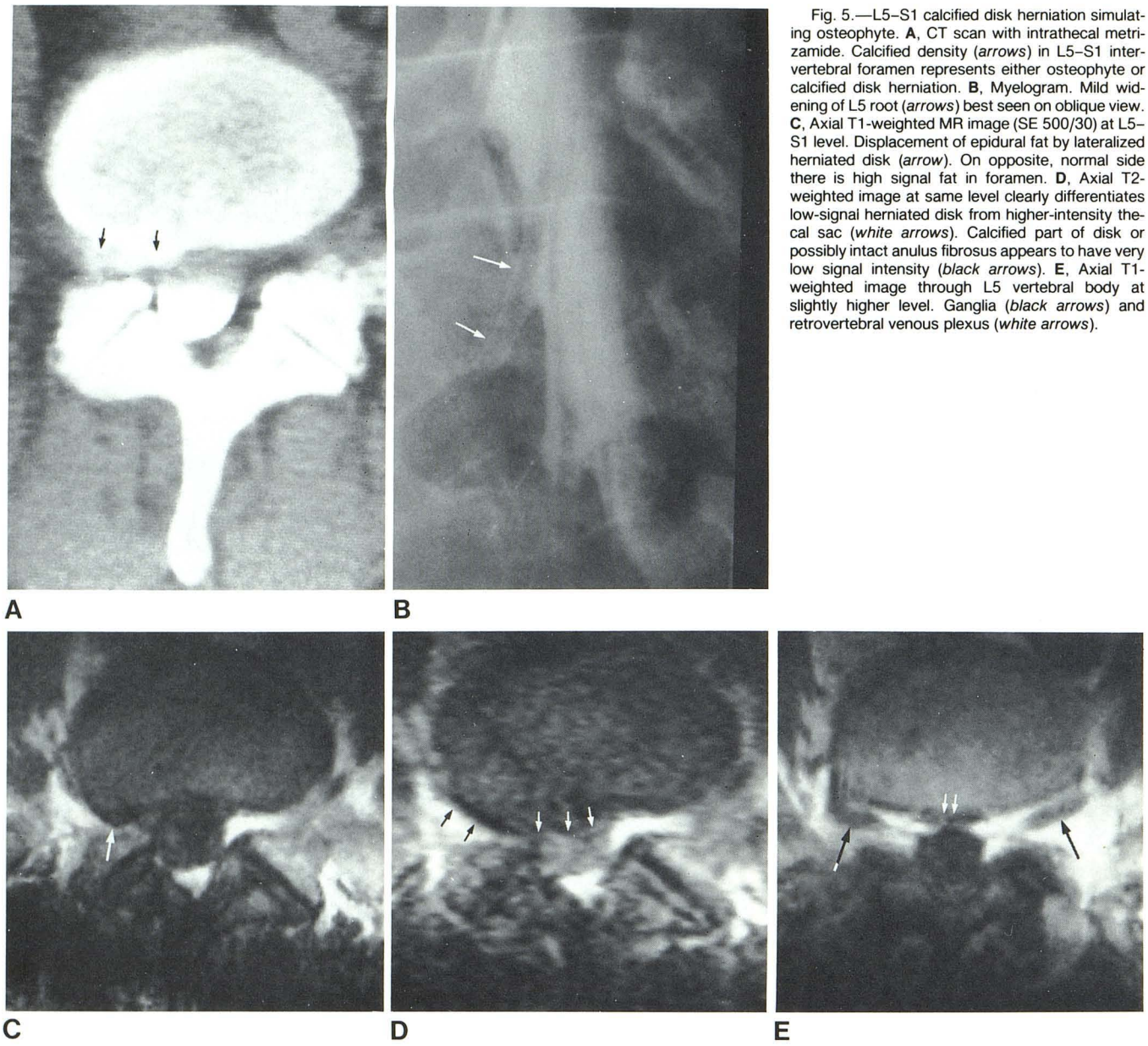

Fig. 5.—L5–S1 calcified disk herniation simulating osteophyte. **A**, CT scan with intrathecal metrizamide. Calcified density (*arrows*) in L5–S1 intervertebral foramen represents either osteophyte or calcified disk herniation. **B**, Myelogram. Mild widening of L5 root (*arrows*) best seen on oblique view. **C**, Axial T1-weighted MR image (SE 500/30) at L5–S1 level. Displacement of epidural fat by lateralized herniated disk (*arrow*). On opposite, normal side there is high signal fat in foramen. **D**, Axial T2-weighted image at same level clearly differentiates low-signal herniated disk from higher-intensity thecal sac (*white arrows*). Calcified part of disk or possibly intact anulus fibrosus appears to have very low signal intensity (*black arrows*). **E**, Axial T1-weighted image through L5 vertebral body at slightly higher level. Ganglia (*black arrows*) and retrovertebral venous plexus (*white arrows*).

characteristic appearance as an extension of the nucleus pulposus against the epidural fat, against the thecal sac, or into the intervertebral foramen (fig. 3A). In one case of a surgically proven disk herniation with an associated extruded fragment, the herniation appeared contiguous with the nucleus pulposus. The fragment, however, was not clearly demonstrated by either MR or CT (fig. 4).

Because of the 5 mm slice thickness, it was sometimes difficult to optimally assess asymmetric disk bulging or herniation on the sagittal views. Furthermore, the degree of focality, which is the major radiographic feature differentiating disk bulge from herniation, was not well assessed on the sagittal views. For these reasons, transverse images were obtained in all cases. The transverse images were routinely angled parallel to the affected disk level. This was achieved by MR in cases where the CT gantry could not be sufficiently angulated, for example, at the L5–S1 level (fig. 1B). Although asymmetry or bulging of herniated disks was best assessed on transverse images, signal-intensity changes characteristic of disk degeneration were best assessed on sagittal images since several disk levels could be compared on a single image.

T1-weighted images generally provided optimal anatomic detail and superb tissue contrast between the herniation, epidural fat, and nerve roots. However, the T2-weighted images occasionally provided better delineation of the disk from the thecal sac, particularly when there was a paucity of epidural fat (fig. 5).

In the two patients with calcified herniations, MR demonstrated low-intensity areas within the herniations, particularly on T2-weighted images (figs. 1G and 5D). However, the

extent of these low-intensity areas was less than that of the corresponding high-density areas of calcification seen on CT.

All 19 herniations were demonstrated well by MR. In one patient it was difficult to determine by CT whether foraminal narrowing was secondary to a vertebral body osteophyte or a calcified herniated disk. Because of the continuity of the intervertebral disk with the herniated part, this distinction could be made on MR (fig. 5C).

Discussion

We have shown that high-resolution surface-coil MR imaging of the lumbar spine has the ability to demonstrate and characterize disk herniation with spatial resolution comparable to that of CT and myelography. The capability of MR to evaluate the lumbar spine with high spatial resolution is a benefit of the high S/N ratio achievable by the surface-coil technique.

Surface coils provide two advantages over conventional whole-body saddle coils. First, because of the small size of the surface coil, its limited field of view, and its proximity to the area being imaged, signal is high and noise is low [10]. The S/N ratio is more than three to five times greater than we have achieved with a whole-body saddle coil using comparable slice thickness and in-plane resolution. To achieve a section thickness, in-plane resolution, and S/N ratio equivalent to those achieved in this study using a surface coil, image acquisition times using our body coil would have to be on the order of hours instead of minutes. Second, surface coils are not affected by artifacts caused by respiratory, bowel, and vessel motion. Whole-body coils allow propagation of those artifacts throughout the image, including the spine. These artifacts become very prominent when small pixel sizes are used for high-resolution studies. The sensitivity of surface coils falls with distance from the coil, so that motion of abdominal structures outside the "field of view" does not degrade the images of the spine.

MR has the advantages of both CT and myelography. As with CT, tomographic cross-sectional MR images are ideally suited for demonstrating lateral disk abnormalities. As with myelography, MR has the capacity to image the entire lumbar spine simultaneously on sagittal images. MR also has the advantage of being completely noninvasive, as no contrast material needs to be introduced and no ionizing radiation is used.

Compared with CT, MR was considerably less able to demonstrate calcification of the herniated nucleus pulposus. However, the presence of calcification can be suggested by regions of decreased signal intensity on both T1- and T2-weighted images.

Although the MR slice thickness and in-plane resolution in our study were slightly inferior to those achievable by current-generation CT scanners, this was compensated for by the capacity to scan in two approximately orthogonal plane orientations. Thus, where a question of partial-volume averaging was raised in the transverse scans, the high in-plane resolution of the sagittal images permitted optimal evaluation. This capacity of MR to demonstrate continuity of the herniation with the nucleus pulposus on the sagittal images permitted easy recognition of herniation or disk bulging.

Total MR examination times in our study were only slightly greater than total CT examination times. However, with improvements in surface-coil design and gradient hardware, we anticipate that at least a further two-fold improvement in S/N ratio for equivalent slice thickness and in-plane resolution will be achieved. This will permit a reduction by a factor of four in total scanning time or, alternatively, reduction in slice thickness and in-plane resolution to reduce partial-volume averaging. In fact, though the 5 mm slice thickness used in our study was generally satisfactory, 3 mm thick slices or smaller would be preferable. In addition, the surface coil is probably best used in a receive-only configuration, rather than the transmit-receive configuration used in our study. This would eliminate the "null" signal bands evident in these images (fig. 3A) resulting from a nonuniform RF field.

Our results demonstrate for the first time that MR imaging can be a practical alternative to CT and myelography in the detection and characterization of lumbar disk herniation. It is anticipated that with further technical improvements and larger clinical trials, surface-coil MR imaging will become established as the procedure of choice for MR imaging of lumbar disk disease.

ACKNOWLEDGMENTS

We thank Paul Beaulieu, Karin Elmden, Rita Zollo, Marlene Bolster, and DeeDee Correia for assistance in patient imaging and Lynda Bessette for manuscript preparation.

REFERENCES

1. Chafetz NI, Genant HK, Moon KL, Helms CA, Morris JM. Recognition of lumbar disk herniation with NMR. *AJNR* **1984**;5:23–26, *AJR* **1983**;141:1153–1156
2. Han JS, Kaufman B, El Yousef SJ, et al. NMR imaging of the spine. *AJNR* **1983**;4:1151–1159, *AJR* **1983**;141:1137–1145
3. Modic MT, Pavlicek W, Weinstein MA, et al. Magnetic resonance imaging of intervertebral disk disease: clinical and pulse sequence considerations. *Radiology* **1984**;152:103–111
4. Modic MT, Weinstein MA, Pavlicek W, et al. Nuclear magnetic resonance imaging of the spine. *Radiology* **1983**;148:757–762
5. Edelman RR, Saini S, Wismer G, et al. Oblique magnetic resonance imaging of the body. Presented at the annual meeting of the Radiological Society of North America, Washington, DC, November **1984**
6. Dinsmore RE, Wismer GL, Levine RA, Okada RD, Brady TJ. Magnetic resonance imaging of the heart: positioning and gradient angle selection for optimal imaging planes. *AJR* **1984**;143:1135–1142
7. Kneeland JB, Knowles RJ, Cahill PT. Magnetic resonance imaging systems: optimization in clinical use. *Radiology* **1984**;153:473–478
8. Crooks LE, Hoenninger J, Arakawa M, et al. High resolution magnetic resonance imaging. *Radiology* **1984**;150:163–171
9. Peterson HO, Kieffer SA. Radiology of non-mass lesions in the spinal canal. *Semin Roentgenol* **1972**;7:260–276
10. Axel L. Surface coil magnetic resonance imaging. *J Comput Assist Tomogr* **1984**;8:381–384